Results in Physics 43 (2022) 106081

Contents lists available at ScienceDirect

Results in Physics

journal homepage: www.elsevier.com/locate/rinp

Thermosolutal natural convective transport in Casson fluid flow in star corrugated cavity with Inclined magnetic field

Imtiaz Ali Shah [a], S. Bilal [a], Arshad Riaz [b,*], ElSayed M. Tag El-Din [c], M.M. Alqarni [d], Haneen Hamam [e]

[a] Department of Mathematics, AIR University, Sector E-9, Islamabad, Pakistan
[b] Department of Mathematics, Division of Science and Technology, University of Education, Lahore 54770, Pakistan
[c] Faculty of Engineering and Technology, Future University in Egypt New Cairo 11835, Egypt
[d] Department of Mathematics, College of Sciences, King Khalid University, Abha 61413, Saudi Arabia
[e] Mathematics Department, Umm Al-Qura University, Makkah 24382, Saudi Arabia

ARTICLE INFO

Keywords:
Thermal and solutal convection
Casson fluid
Star corrugated cavity
Inclined MHD, FEM

ABSTRACT

Diffusion mechanism generated because of thermal and solutal buoyant forces in star corrugated cavity filled with Casson liquid is envisioned in this study. Magnetic field making angle of inclination with enclosure is also taken into account. Rectangular plate with isothermal and isoconcentration distributions is installed. To measure optimized variation in associated distributions all the extremities of enclosure are kept at cold temperature and zero concentration. Governing equations are modelled by incorporating conservation laws. After then, complexly formulated model equations and their associated boundary constraint are change in dimensionless structure by obliging variables. Numerical simulations are performed by opting finite element based commercial software renowned as COMSOL. Domain is discretized in the form of triangular and rectangular elements by executing hybrid meshing. Afterwards, non-linear solver (PARADISO) is capitalized to handle system of non-linear equations. Mesh independence test is carried out to assure credibility of conducted simulations. Comparison of results with published literature is also displayed. Graphical and tabular representation describing change is associated fields (velocity, temperature and concentration) against wide range of involved parameters. Change in kinetic energy along with average Sherwood and Nusselt number against different magnitudes of Casson parameter is divulged through tables.

Introduction

Diffusion transport mechanism in liquids resulting due to thermal and species concentration changes is denoted as thermosolutal convection. Depending on orientation of gradients existed during the flow in enclosures multiple type of diffusions occurs. Among these thermosolutal convection has received promising applications in diversified fields, e.g. thermal engineering, geophysics and astrophysics. In addition, in geothermal phenomena the role of stratification produced due to variation in intensification of temperature and solutal distributions is highly beneficial in crystal growth, oceanography and management of water reservoirs. Some highly recommendable utilizations related to current topic are encapsulated in [1–11]. Beghein et al. [12] carried out analysis on effectiveness of assisting and opposing solutal buoyancy force on steady state thermosolutal convection in air enclosed in square cavity. Numerical simulations were performed by Gobin and Bennacer [13] to contemplate multicellular flow structure of binary fluid contained in an enclosure with imposition of horizontal thermosolutal differences. Examination about diffusion under joint influence of inertial and thermal/solutal buoyancy forces was divulged by Aimiri et al. [14]. Deposition of nanocomposite on electrodes by varying mass diffusions with static magnetization was delineated by Zhou et al. [15]. A comprehensive analysis on effect of variation in aspect ratio of annular region on heat mass transport in domain was visualized by Chen et al. [16]. Kefayati and his coauthors [1,17–19] performed computational simulations by LBM method to explicate thermal and solutal diffusivity pehnomenon in closed domains with numerous physical aspects. In addition, for the sake of interest of readers and keeping essence of work in mind some related work is provided in refs. [11,20–25].

Matherials possessing elastic characterisitcs and requires specific

* Corresponding author.
E-mail address: arshad-riaz@ue.edu.pk (A. Riaz).

https://doi.org/10.1016/j.rinp.2022.106081
Received 15 August 2022; Received in revised form 10 October 2022; Accepted 31 October 2022
Available online 1 November 2022

threshold of stress for producing deformation is recongnized as visco-elastic liquids. The effectiveness and appliance of these materials are observed in daily life products e.g. Combination of paints with polymers and solver is good use of these materials and obliged in buildings for renovations along with fabrication of complexed surfaces. Other than this viscoelastic materials also characterizes the features of blood and efficiently used in DNA replication process. Packaging of drugs and refinement of curde oil are also the examples which describes employment of these materials. For comprehsensive response of viscoelastic materials against yielding stress at high shearing viscosity formulating mathematical framework was demarcated by Casson [26]. After this an extensive work on Casson fluid with multiple physical aspects are discussed like Rao et al. [27] delineated impact of surface drag force on yielding stress and found that for infinite shear stress at surface the fluid will behave as solid. Bird et al. [28] analyzed rheology of materials with yields by utilizing Casson fluid model and measured driving gradients beyond and below the critical stress. Some research studies descrbing the importance and characteristics of viscoelastic materials by incorporating Casson model is disclosed in refs. [29–33].

Transportation of fluid regimes under the implementation of transverse magnetization make them more potentially more applicable in different governing problems rather in absence. The liquids which polarizes and respond to magnetic field are called as electrically conducting. In addition, these magnetized liquids store extra energy due to polarization and thus employed in numerous engineering systems like reactor frameworking, coolant in reactors, packaging of instruments, growths of crystals, solar panels and so forth. Garandet et al. [34] demonstrated stratified flow of water in rectangular cavity generated by magnetization and buoyant forces. Rudrariah et al. [35] found decrement in momentum and thermal diffusivities of liquid by providing magnetization. Scaling procedure was opted by Hadid et al. [36] to defined dimensionless representation of magnetic strength parameter for description of flow in different physical circumstances. Tagawa and Ozoe [37] delineated convective flow of mettalic liquid in a cube by applying static magnetic field and measure depreciation in momentum and enhancement in thermal field against Hartmann number. Problem formulation for single phase nanofluid flow in wavy cavity for wide range of Hartmann number was adumbrated by Sheremet et al. [38]. Kifayati and his coresearchers [39,40] comprehended changes in convective flow of liquids in different shaped cavities by executing unfiormly palced magnetic source. Latest developments on convective flow of ordinary and nanofluid flow in confined geometries by measuring diffusion with physical prospectives of magnetic field and installement of objects are encapsulated in [41–48].

It is prompted from accessible literature review and analyzing extensive appearance of thermally and solutaly convective diffusion transport in diversified processes this effort is made. Subsequently, so far examination of above said physical features are not interrogated even with viscous liquid. But in this document we have performed advance study by obliging Casson liquid in star enclosure with corrugations and with employment of magnetic field with inclination. So, the prime consent of all author is on to fill this breach. For this purpose a rectangular fin is installed by providing constant heat and mass distributions. Additonally, results are validated by constructing limitized situation for present case study and compared with existed results.

Formualtion of problem

Description statement

A star shaped enclosure with corrugation filled with laminar and incompressible flow of Casson liquid is taken into account. A rectangular fin of unit length by providing constant temperature and concentration distribution is also installed. Fluid density is assumed to be the function temperature and concentration gradients due to which convection in domain is generated. Inclining magnetic field of uniform strength forming angle γ is considered. Graphical visualization of domain is displayed in Fig. 1.

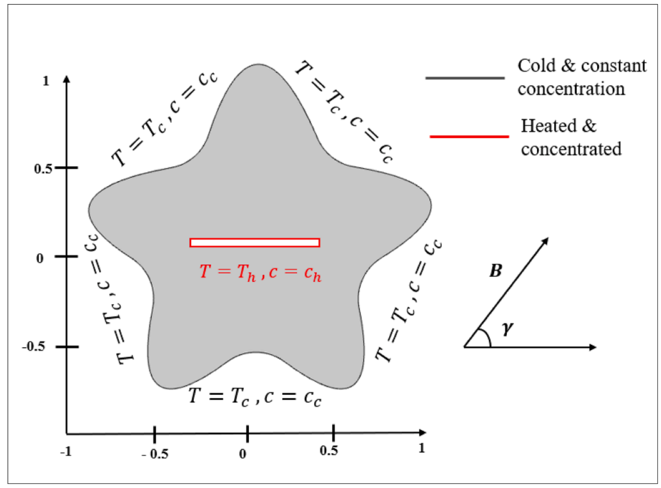

Fig. 1. Graphical description of domain.

Constitutive equations

A Casson fluid model constitutive equation describing the connection between stress and deformation rate is mentioned below [48].

$$\sqrt{\tau^*} = \sqrt{\mu\dot{\gamma}^*} + \sqrt{\tau_0^*}, for \tau^* \geq \tau_0^*,$$

$$\dot{\gamma}^* = 0, for \tau^* \leq \tau_0^* \tag{1}$$

here, τ^* $and \tau_0^*$ represent shearing and yielding stresses.

The govering transport equations for considered problem is as follows [36].

$$\frac{\partial u}{\partial x} + \frac{\partial v}{\partial y} = 0 \tag{2}$$

$$\rho\left(u\frac{\partial u}{\partial x} + v.\frac{\partial u}{\partial y}\right) = -\frac{\partial p}{\partial x} + \mu\left(1+\frac{1}{\beta}\right)\left(\frac{\partial^2 u}{\partial x^2} + \frac{\partial^2 u}{\partial y^2}\right) + \Lambda_x \tag{3}$$

$$\rho\left(u\frac{\partial v}{\partial x} + v\frac{\partial v}{\partial y}\right) = .-\frac{\partial p}{\partial y} + \mu\left(1+\frac{1}{\beta}\right)\left(\frac{\partial^2 v}{\partial x^2} + \frac{\partial^2 v}{\partial y^2}\right) + \Lambda_y \tag{4}$$

$$u\frac{\partial T}{\partial x} + v\frac{\partial T}{\partial y} = \alpha_e\left(\frac{\partial^2 T}{\partial x^2} + \frac{\partial^2 T}{\partial y^2}\right) \tag{5}$$

$$u\frac{\partial c}{\partial x} + v\frac{\partial c}{\partial y} = D\left(\frac{\partial^2 c}{\partial x^2} + \frac{\partial^2 c}{\partial y^2}\right) \tag{6}$$

Here, Λ denotes the forcing factor generated due to magnetization.

After utilizing Boussinesq approximation the forcing factor takes following form.

$$\Lambda_x = \sigma B_0^2\left(v sin\gamma cos\gamma - u sin^2\gamma\right) \tag{7}$$

$$\Lambda_y = \sigma B_0^2\left(u sin\gamma cos\gamma - v cos^2\gamma\right) + \rho g[\beta_T(T - T_c) + \beta_c(c - c_c)] \tag{8}$$

Where, β_T and β_c shows the thermosolutal diffusivites, respectively.

Prescribed wall conditions

$$u = 0, v = 0, T = T_h, c = c_h, \left(-\frac{L}{2} \leq x \leq \frac{L}{2}\right), y = 0 \tag{9}$$

$$u = 0, v = 0, T = T_c, c = c_c, \; -L \le x \le L, \; -L \le y \le L \tag{10}$$

Utilization of below mentioned set of variable for conversion into dimensioless resperesentiton.

$$(X^*, Y^*) = \frac{(x,y)}{L}, (U^*, V^*) = \frac{(u,v)L}{\alpha}, P^* = \frac{pL^2}{\rho\alpha^2}, \theta^* = \frac{T - T_c}{T_h - T_c}, C^* = \frac{c - c_c}{c_h - c_c} \tag{11}$$

$$\alpha_e = \frac{k_e}{(\rho c_p)_f}, Ra = \frac{\rho^2 \beta_T g L^3 \Delta T Pr}{\upsilon^2}, Le = \frac{\alpha_e}{\mathrm{D}}, Ha = BL\sqrt{\frac{\mu}{\sigma}}, Pr = \frac{\nu}{\alpha} \tag{12}$$

Non-dimensional visualtization of transport equations is attained below [48].

$$\frac{\partial U^*}{\partial X^*} + .\frac{\partial V^*}{\partial Y^*} = 0 \tag{13}$$

$$\left(U^* \frac{\partial U^*}{\partial X^*} + V^* .\frac{\partial U^*}{\partial Y^*}\right) = -\frac{\partial P^*}{\partial X^*} + Pr\left(1 + \frac{1}{\beta}.\right)\left(\frac{\partial U^*}{\partial X^*}. + \frac{\partial U^*}{\partial Y^*}\right) + \Lambda_{X^*} \tag{14}$$

$$\left(U^* \frac{\partial V^*}{\partial X^*} + V^* .\frac{\partial V^*.}{\partial Y^*}\right) = -\frac{\partial P^*}{\partial Y^*} + Pr\left(1 + \frac{1}{\beta}.\right)\left(\frac{\partial V.^*}{\partial X^*} + \frac{\partial V^*}{\partial Y^*}\right) + \Lambda_{Y^*} \tag{15}$$

$$U^* \frac{\partial \theta^*}{\partial X^*}. + V^* .\frac{\partial \theta^*}{\partial Y^*} = \frac{.\partial^2 \theta^*}{\partial X^{*2}} + \frac{\partial^2 \theta^*}{\partial Y^{*2}} \tag{16}$$

$$U^* \frac{\partial C^*}{\partial X^*} + V^* \frac{\partial C^*.}{\partial Y^*} = \frac{1}{Le}\left(\frac{\partial^2 C^*.}{\partial X^{*2}} + \frac{\partial^2 C^*}{\partial Y^{*2}.}\right) \tag{17}$$

Where,

$$\Lambda_{X^*} = PrHa^2\left(V^* sin\gamma cos\gamma - U^* sin^2\gamma\right) \tag{18}$$

$$\Lambda_{Y^*} = PrHa^2\left(U^* sin\gamma cos\gamma - V^* cos^2\gamma\right) + RaPr(\theta^* + NC^*). \tag{19}$$

Conditions at boundaries of domain in dimensionless structuring is as under.

$$U^* = 0V^* = 0\theta^* = 1C^* = 1\left(-\frac{1}{2} \le X^* \le \frac{1}{2}Y^* = 0\right) \tag{20}$$

$$U^* = 0V^* = 0\theta^* = 0C^* = 0(-1 \le X^* \le 1 - 1 \le X^* \le 1) \tag{21}$$

Corelations defining local and mean heat and mass fluxes are described below.

$$Nu_{local} = -\left.\frac{\partial \theta^*}{\partial n}\right|_{innerwall}, \tag{22}$$

$$Sh_{local} = -\left.\frac{\partial C^*}{\partial n}\right|_{innerwall}, \tag{23}$$

$$Nu_{avg} = \frac{1}{L}\int_L^1 Nu_{local} dL, \tag{24}$$

$$Sh_{avg} = \frac{1}{L}\int_L^1 Sh_{local} dL. \tag{25}$$

Additionally, globally quantified kinetic energy is shown as under.

$$K.E = \frac{1}{2}\int_\Omega \|U\|^2 \, d\Omega. \tag{26}$$

Compuational scheme

Transport mechanism in fluids in simple confined geometries is easily managed by exact approaches and traditional schemes. But, most of the problems in nature arises is intricate structural designs so previously implemented exact schemes are unable to solve them. For this prupose the analytical approaches are found to be the best for solving these problems. Specifically discussing about the irregular shapes the flow phenomeon is efficiently tackled by versatile method known as finite element method. In this procedure the domain is divided into small portions and variable of interest are computed at element level. Depending on field variables degrees of freedom are computed at different refinement levels as shown in Table 1 and interpolated by utilizing stable element pair. Since, the govering problem discussed here comprises of pressure which is approximated by linear polynomials where as rest of distributions are approximated by quadratic polynomials. Descritization of domain is manifested in Fig. 2 describing hybrid meshing at coarse level with triangular and rectangular elements. Afterwards, system of non-linearized equations are formed and solved by direct solver known as PARADISO. The steps involved in the scheme are presented in Table 1. Convergence criterion adjusted for nonlinear iterations is as follows

Table 1
Meshing at different level of refinements.

Grid	# EL	#DOFs
Extremely coarse	390	2607
Extra coarse	552	3630
Coarser	878	5643
Coarse	1476	9284
Normal	2130	13,189
Fine	3388	20,504
Finer	8092	48,224
Extra fine	20,002	117,161
Extremely fine	27,678	159,379

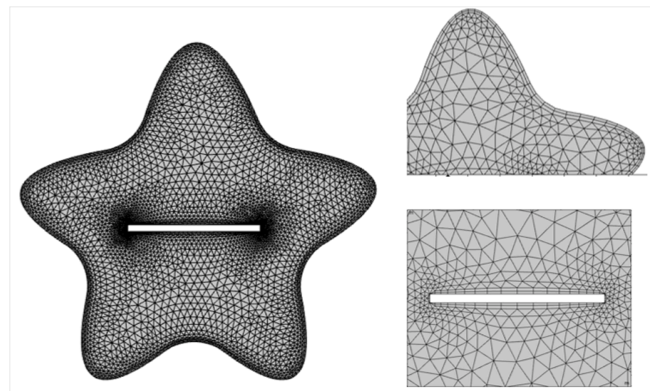

Fig. 2. Element formation in domain at coarser grid.

$$\left|\frac{\chi^{n+1} - \chi^n}{\chi^{n+1}}\right| \langle \, 10^{-6}$$

Where, χ characterizes the general solution component (Fig. 3).

Discretization of equations (Weak Formulation)

Let subspace for $U^*., V^*., \theta^*, C^*$ is $W = \left[H^1(\Omega)\right]^3$ be the test subspaces for pressure is $Q = L^2(\Omega)$. The weak form of the governing equation is given as.

$$\int_\Omega \left(U^* \frac{\partial U^*}{\partial X^*} + V^* .\frac{\partial U^*}{\partial Y^*}\right) w d\Omega + \int_\Omega \frac{\partial P^*}{\partial X^*} w d\Omega + Pr\int_\Omega \left[\left(1 + \frac{1}{\beta}.\right)\left(\frac{\partial U^*}{\partial X^*}. + \frac{\partial U^*}{\partial Y^*}\right) + \Lambda_{X^*}\right] w d\Omega = 0, \tag{27}$$

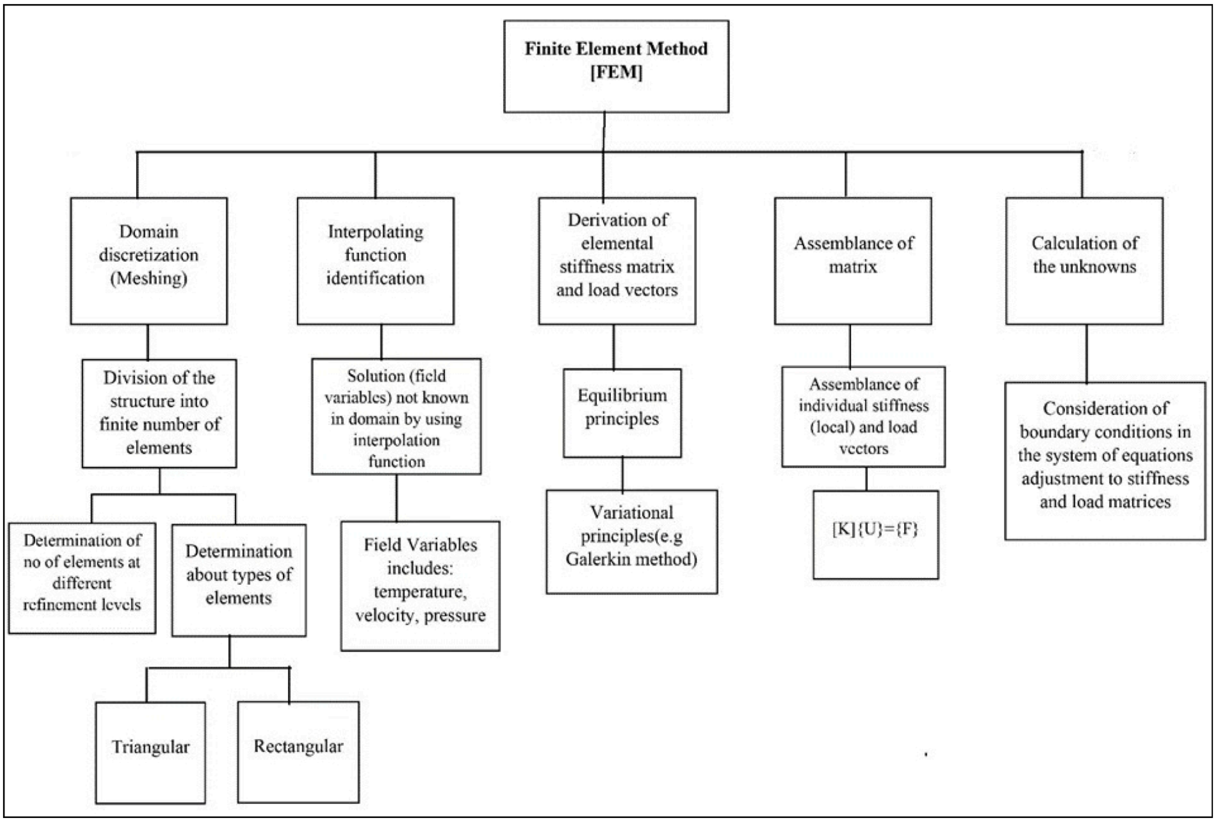

Fig. 3. Diagram representing steps involved in scheme.

$$\int_\Omega \left(U^*\frac{\partial V^*}{\partial X^*} + V^*.\frac{\partial V^*}{\partial Y^*}\right) w d\Omega + \int_\Omega \frac{\partial P^*}{\partial Y^*} w d\Omega + Pr\int_\Omega \left[\left(1+\frac{1}{\beta}.\right)\left(\frac{\partial V^*}{\partial X^*}. + \frac{\partial V^*}{\partial Y^*}\right) + \Lambda_{y^*}\right] w d\Omega = 0 \tag{28}$$

$$U^* \approx U^*{}_h \in W_h V^* \approx V^*{}_h \in \tag{32}$$

$$\theta^* \approx \theta^*{}_h \in W_h$$

$$C^* \approx C^*{}_h \in W_h P^* \approx P^*{}_h \in Q_h$$

$$\int_\Omega \left(U^*{}_h \frac{\partial U^*{}_h}{\partial X^*} + v\frac{\partial U^*{}_h}{\partial Y^*}\right) w_h d\Omega + \int_\Omega \frac{\partial P^*{}_h}{\partial X^*} w_h d\Omega - Pr\int_\Omega \left(1+\frac{1}{\beta}.\right)\left(\frac{\partial^2 U^*{}_h}{\partial X^{*2}} + \frac{\partial^2 U^*{}_h}{\partial Y^{*2}}\right) w_h d\Omega + \Lambda_{X^*} \tag{33}$$

$$\int_\Omega \left(U^*{}_h \frac{\partial V^*{}_h}{\partial X^*} + V^*{}_h \frac{\partial V^*{}_h}{\partial Y^*}\right) w_h d\Omega + \int_\Omega \frac{\partial P^*{}_h}{\partial X^*} w_h d\Omega - Pr\int_\Omega \left(1+\frac{1}{\beta}.\right)\left(\frac{\partial^2 U^*{}_h}{\partial X^{*2}} + \frac{\partial^2 U^*{}_h}{\partial Y^{*2}}\right) w_h d\Omega + \Lambda_{Y^*} \tag{34}$$

Integral form of mass conservation equation is described as under.

$$\int_\Omega \left(\frac{\partial U^*}{\partial X^*} + \frac{\partial V^*}{\partial Y}\right) q d\Omega = 0 \tag{29}$$

$$\int_\Omega \left(U^*\frac{\partial \theta^*}{\partial X^*} + V^*\frac{\partial \theta^*}{\partial Y^*}\right) w d\Omega - \int_\Omega \left(\frac{\partial^2 \theta^*}{\partial \theta^{*2}} + \frac{\partial^2 \theta^*}{\partial Y^{*2}}\right) w d\Omega = 0, \tag{30}$$

$$\int_\Omega \left(U^*\frac{\partial C^*}{\partial X^*} + V^*\frac{\partial C^*}{\partial Y^*}\right) w d\Omega - \frac{1}{Le}\int_\Omega \left(\frac{\partial^2 \theta^*}{\partial \theta^{*2}} + \frac{\partial^2 \theta^*}{\partial Y^{*2}}\right)$$

Continuous solutions is approximated by discrete ones in the finite dimensional sub-spaces.

$$\int_\Omega \left(\frac{\partial U^*{}_h}{\partial X^*} + \frac{\partial V^*{}_h}{\partial Y^*}\right) q d\Omega = 0, \tag{35}$$

$$\int_\Omega \left(U^*{}_h \frac{\partial \theta^*{}_h}{\partial X^*} + V^*{}_h \frac{\partial \theta^*{}_h}{\partial Y^*}\right) w_h d\Omega - \int_\Omega \left(\frac{\partial^2 \theta^*{}_h}{\partial X^{*2}} + \frac{\partial^2 \theta^*{}_h}{\partial Y^{*2}}\right) w_h d\Omega = 0, \tag{36}$$

$$\int_\Omega \left(U^*{}_h \frac{\partial C^*{}_h}{\partial X^*} + V^*{}_h \frac{\partial C^*{}_h}{\partial Y^*}\right) w_h d\Omega - \int_\Omega \left(\frac{\partial^2 C^*{}_h}{\partial X^{*2}} + \frac{\partial^2 C^*{}_h}{\partial Y^{*2}}\right) w_h d\Omega = 0, \tag{37}$$

In matrix representation.

Table 2
Mesh independence for mean heat and mass fluxes.

Grid	Nu_{avg}	Sh_{avg}	K.E.
Extremely coarse	7.6644	1.6335	545.91
Extra coarse	7.7575	1.5015	552.88
Coarser	7.8530	1.3531	558.65
Coarse	8.1099	1.1601	551.95
Normal	8.2137	1.1145	549.11
Fine	8.3375	1.0528	547.71
Finer	8.6075	0.97155	545.58
Extra fine	8.7525	0.94589	543.65
Extremely fine	8.7504	0.94173	543.67

Table 3
Conformity of results for Nusselt number against different value of.β.

β	Shafqat et al. [48]	Present
0.1	2.38986	2.39023
1	3.81194	3.81168
5	4.27587	4.27511
10	4.35556	4.35470

$$\begin{bmatrix} Pr.L_h+N(U^*{}_h,V^*{}_h) & 0 & B_1 & 0 \\ 0 & Pr.L_h+N_h(U^*{}_h,V^*{}_h) & B_2 & -RaPrM_h \\ B_1^T & B_2^T & 0 & 0 \\ 0 & 0 & 0 & L_h+N_h(U^*{}_h,V^*{}_h) \\ & 000L_h+N_h(U^*{}_h,V^*{}_h) & & \end{bmatrix} \begin{bmatrix} U^* \\ V^* \\ P^* \\ \theta^* \\ C^* \end{bmatrix} = \begin{bmatrix} F_1 \\ F_2 \\ F_3 \\ F_4 \\ F_5 \end{bmatrix} \tag{38}$$

which can be written as:$\boldsymbol{A\xi} = \boldsymbol{F}$

$\boldsymbol{L_h}$: Discrete Laplace matrix, $\boldsymbol{N_h}$: Non-linear convection matrix, $\boldsymbol{M_h}$: Mass matrix, $\boldsymbol{\xi}$: Solution vector, $\boldsymbol{F}$: Right hand side after implementation of boundary condition. To compute the solution, this non-linear system is iterated till a specified convergence criterion is met. The

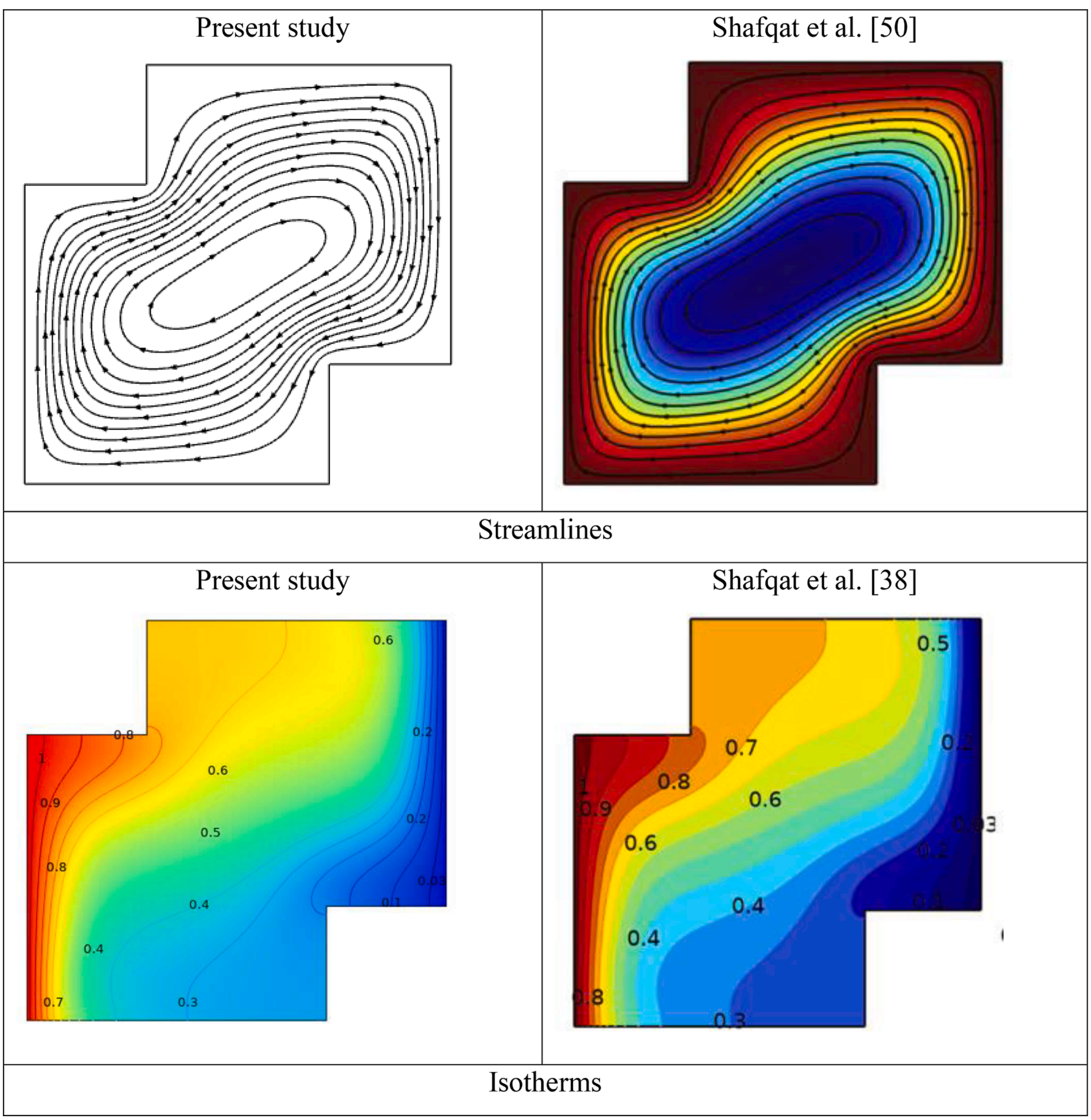

Fig. 4. Stream lines and isothermal contours presentation to depict agreement of results.

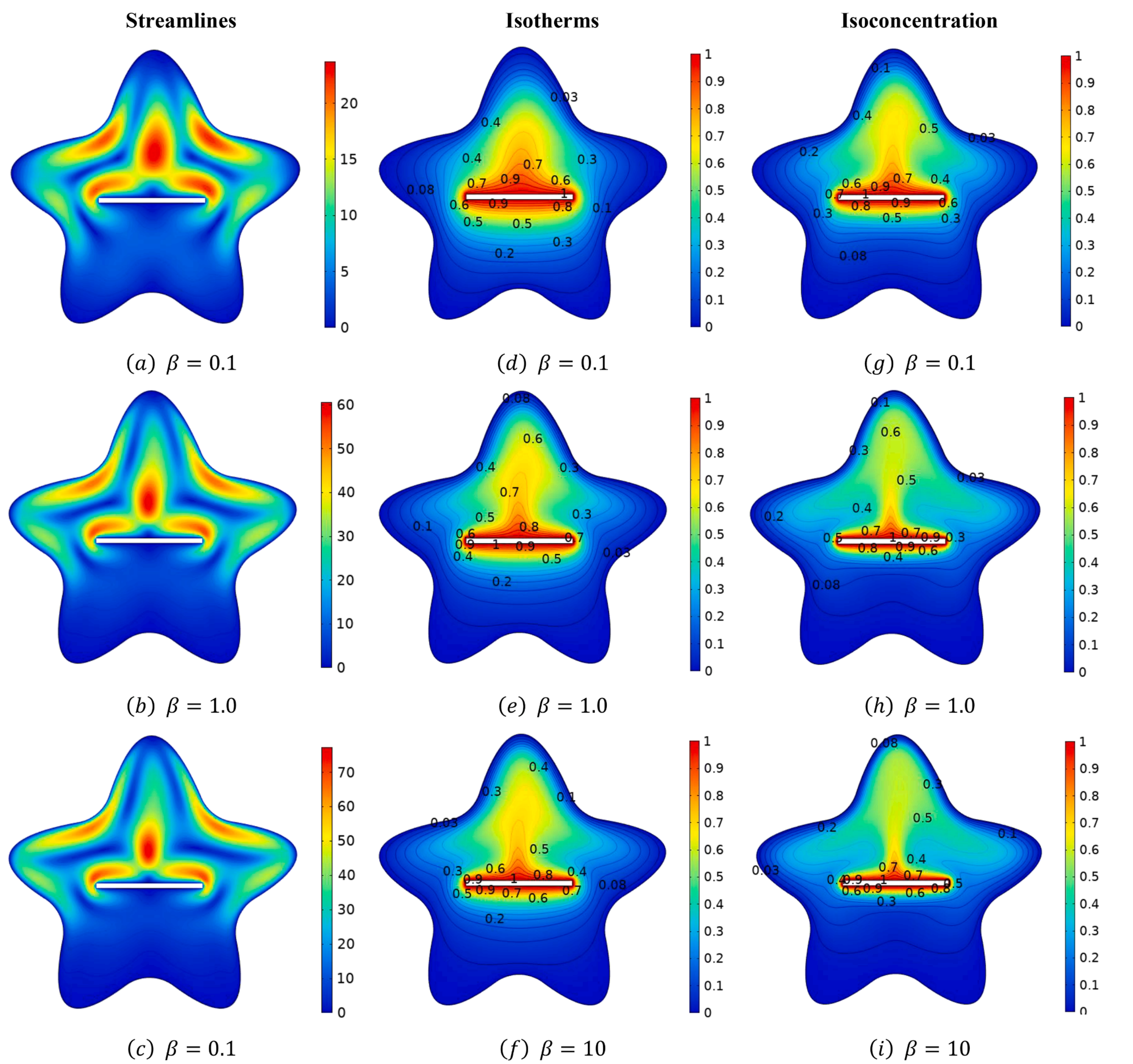

Fig. 5. Variatation in velocity, thermal and solutaly concentrated fields against (β).

nonlinear iterations are stopped when the residual is dropped by10^{-6}.

Mesh independence test

Efficiency of implemented numerical scheme is checked in Table 2 by performing mesh independence test by changing refinement levels and by fixing all involved physical parameters. Estimation about global quantities like Kinetic energy, Nusselt and Sherwood numbers are measured and found complete match between level 8 and 9.

Resutls validation

Crediblity of presently computed finding is assured by making match with results presented by Shafqat et al. [48] as shown in Table 3. Here, heat flux coefficient is measured against Casson parameter and strong agreement between available and current studies is found. This agreement of results is graphically visualized in Fig. 4.

Results and discussion

This portion is presented to adumbrate the impression of involved physical parameters on associated distribution via streamlines, countour plots for temperature and species depositon. Intially, system of governing equations are modelled in the form of PDEs and solved by implementing finite element approach. To enrich attraction in current work for engineers some valuable globaly and localy distributed quantities like kinetic energy, Nusselt number and Sherwood numbers are also measured.

Chang in velocity, themal and solutal profiles versus wide range of Casson parameter (β) is elaborated in Fig. 5. Description about deviation in flow of non-Newtonian fluid against (β) is divulged in Fig. 5(a-c). Since by increasing (β) the flow behavior of considered non-Newtonian approaches towards Newtonian fluid so velocity field is found to decreasing function of (β). Thus, at lower magnitude of (β) stream patterns are more than in case of $\beta = 10$. Response of temperature distribution against (β) is manifested in Fig. 5(d-f). It is seen that positive

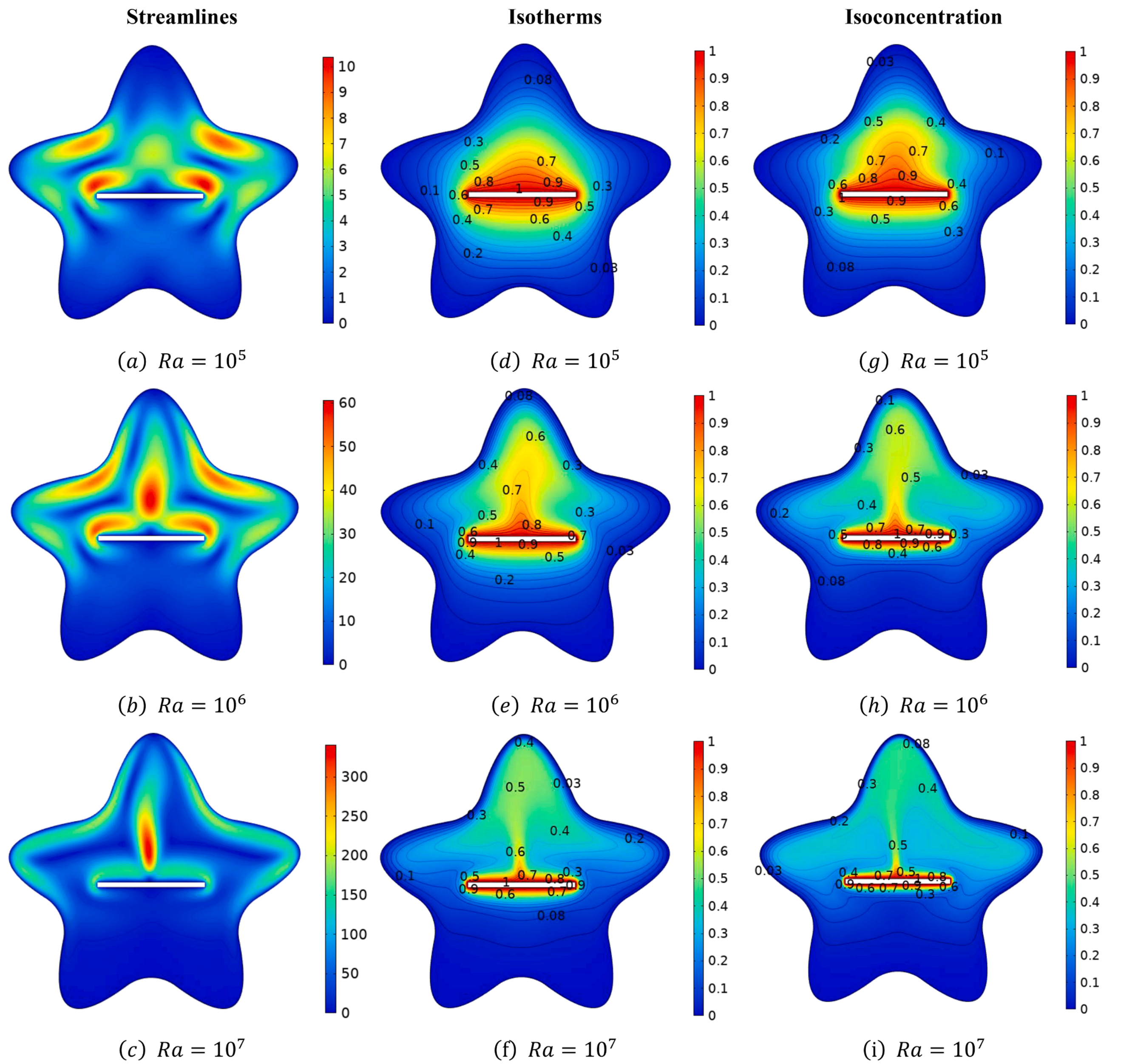

Fig. 6. Variatation in velocity, temperature and solutaly concentrated fields against Rayleigh number (Ra).

trend in magnitude of temperature is observed at $\beta =\ 10$because velocity at this magnitude of (β) is high than at $\beta = 0.1$. So, the average kinetic energy is also higher which describes the temperature distribution. Influence of Casson parameter (β) on species mass distribution is interpreted in Fig. 5(g-i). At lower values of (β) dominance in accumulation of particles is attained because viscosity of fluid is more rather than in case of $\beta = 10$. Additonally, due to provison of constant mass distribution at rectangular plate more solutal convective potential is generated in upper reigon of enclosure.

Wide range of Rayleigh number (Ra) is opted to discuss its effectiveness on velocity, temperature and concetrataion field as shown in Fig. 6(a-i). Posotive trend in magnitude of stream function assigned for comprehension of velcotiy field is evaluated against (Ra) in Fig. 6(a-c). It is because of the fact that (Ra) has direct relation with temepature gradient between cold and hot portions in domain and has inverse relation with viscosity. So, by uplifting (Ra) viscosity of fluid decreases and momentum diffusivity of particles enriches. Description about effectiveness of (Ra) on thermal profile is discussed in Fig. 6(d-f). Enhancement in temepature of fluid is attained due to generation of extensive temperature difference between cold and hot reigons of enclosure. Due to this fact thermal convective potential is generated which mount the role of thermal buoyancy force and thus as an outcome temperature of fluid upsurges. Resposne of solutal concentration versus (Ra) is measured in Fig. 6 (g)-(i). It is revealed that concentrataion of fluid is extensive for high values of (Ra) This is justified by the fact that at lower magnitude of (Ra) fluid accumulates more due to production of minute concentration differences and contrary to it the concentration field exceeds.

Role of magnetic field parameter (Ha) on momentum, thermal and solutally conentrated profiles are examined in Fig. 7(a-i). Since the appliance of magnetization to the flow generates resistive force to the fluid which causes reduction in velocity field and produces laminar field. So, it is found in Fig. 7(a-c) that at higher magnitude i.e. $\mathrm{Ha} = 60$ lower magnitude of velocity is attained. Similarly, decrementing trend in temperature distribution delineated from isothermal conoturs is determined in fig. (d-f). It is due to the reason that by incrementing (Ha)

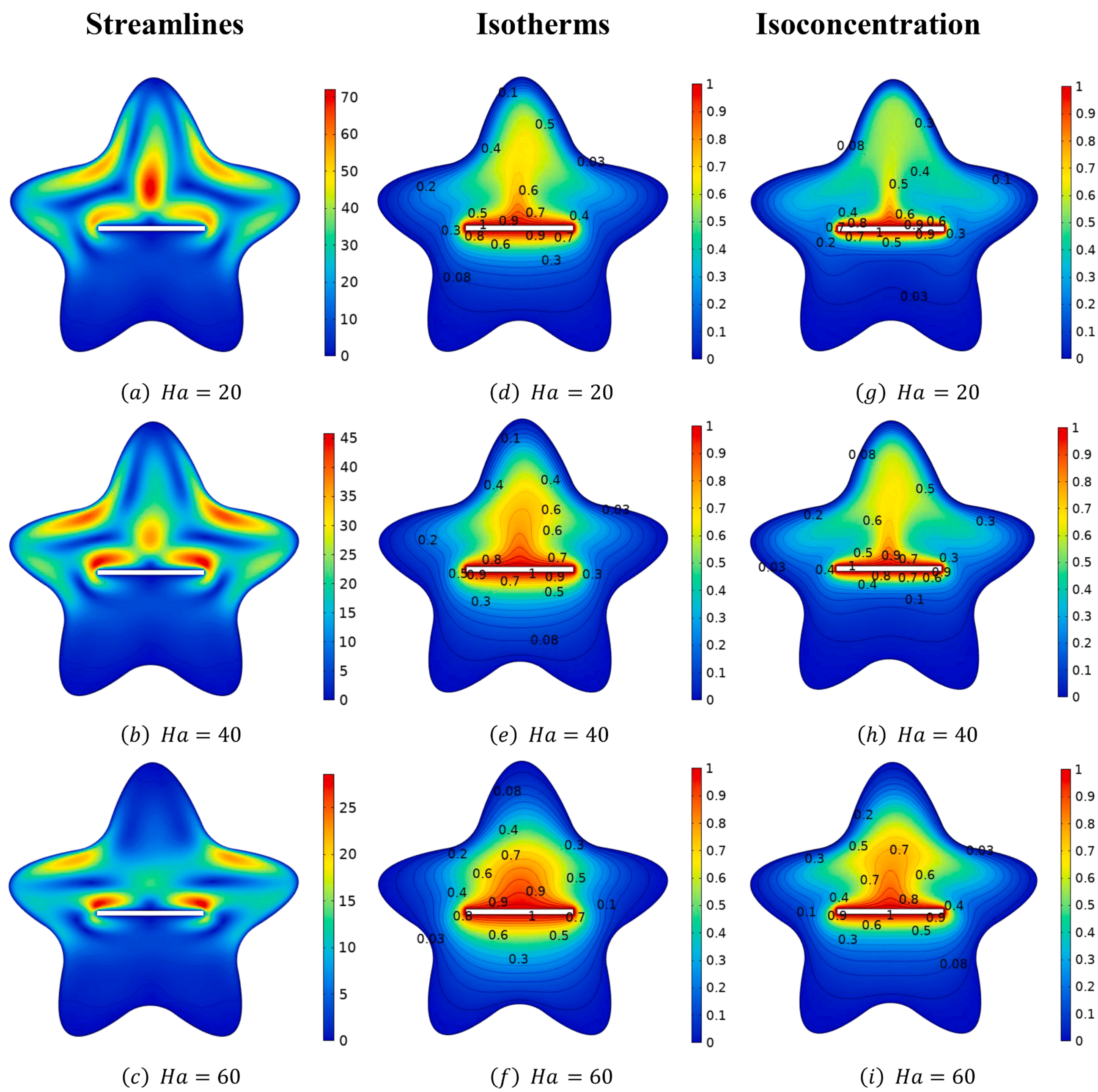

Fig. 7. Variatation in velocity, thermal and solutaly concentrated fields against Hartmann number (*Ha*).

average kinetic energy of particles deceeds which as an outcome diminishes the temperature of fluid. Since, viscosity of fluid shows increasing trend against (Ha) due to production of Lorentz resisitive force so the particles accumulates and concentration field mount which is evidenced in Fig. 7(g-i).

Exploration about implication of Lewis number (Le) on velocity, thermal and solutaly concentrated fields is manifested in Fig. 8(a-i). No significant changes in velocity and temperature fields are found against (Le) in Fig. 8(a-f) because no direct correspondence with momentum and thermal diffusivities exist. Whereas, in view of concentration distribution it depreciates against increasing values of Lewis number (Le) as shown in Fig. 8(g-h). In addition, solual boundary layer near the rectangular plate where constant concentration distribution is capatilzed becomes thinner at Le $= 10$.

Table 4 enumerates numerical data examining variation in (Nu_{avg}) and (Sh_{avg}) against (Ha) and (β). At Ha $= 0$ maximum magnitude of heat flux coefficient is attained whereas lowest values of mass flux is attained and contrary aspects are attained at Ha $= 100$ for both physical quantiites. This is justified by the fact that at Ha $= 0$ no magnetic field is present which allow the particles to move freely in the domain due to which average kinetic energy enhances and associated heat flux rate uplift whereas the concentration of fluid particles does not accumulates.

Description about deviation in kinetic energy for wide range of Hartmann number (Ha) and Casson parameter (β) is explicated in Table 5. It is found that kinetic energy at $\beta = 10$ and in the absence of magnetic field is increased by 17.5 times more than for $\beta = 0.1$. The reason behind this phenomeon is that the Casson fluid approaches towards Newtonian case for higher magnitude and viscosity of fluid becomes constant. So, the kinetic energy of particles raises and additionally no magnetic field is present in this case so no resistive forces are generated.

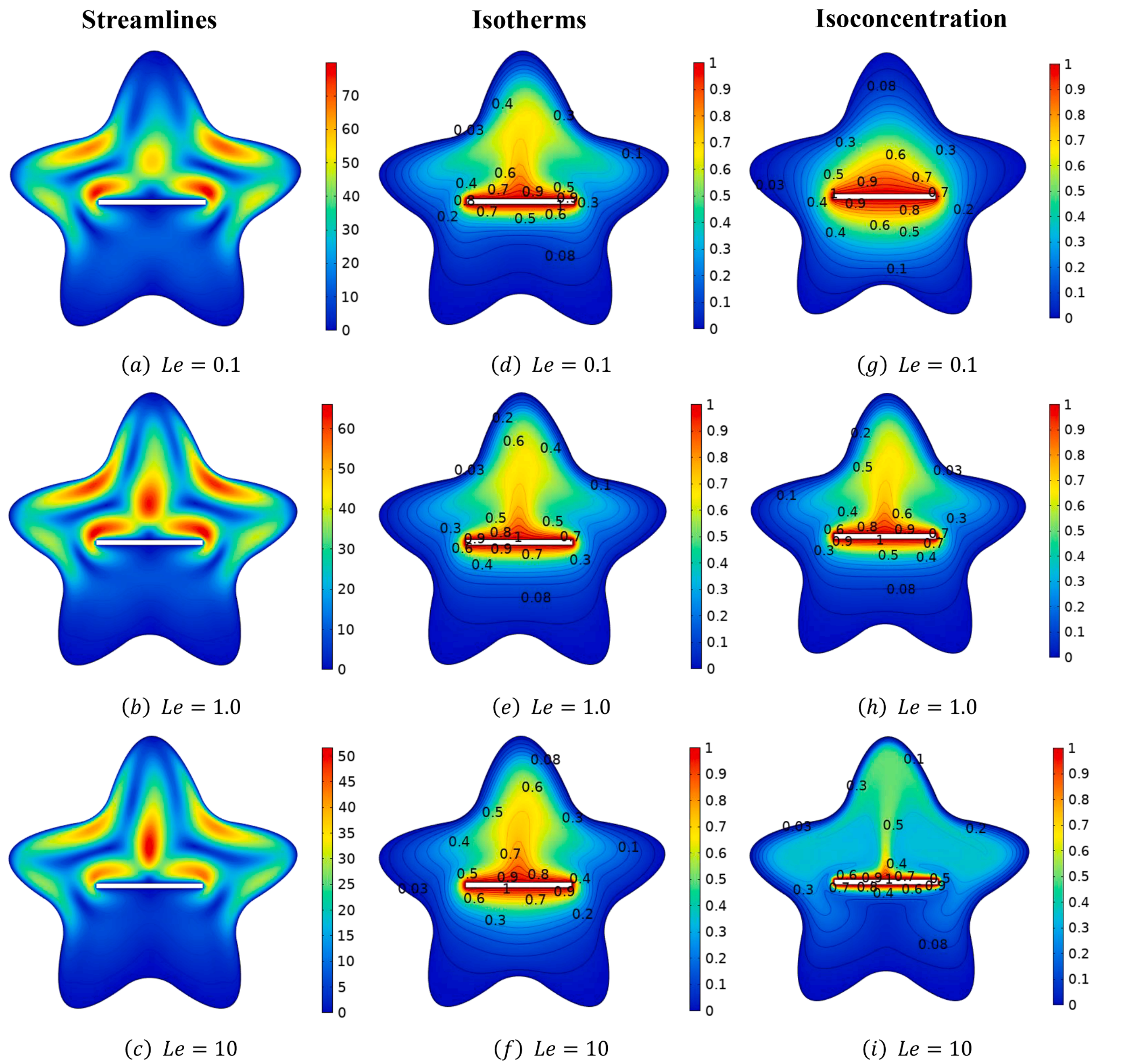

Fig. 8. Variatation in velocity, thermal and solutaly concentrated fields against Lewis number (Le).

Table 4
Variation in average Nusselt and Sherwood numbers against (β) and (Ha).

Nu_{avg}				Sh_{avg}		
Ha	$\beta=0.1$	$\beta=1$	$\beta=10$	$\beta=0.1$	$\beta=1$	$\beta=10$
0	5.5438	8.6040	9.8667	0.50247	0.69399	1.86590
25	5.3113	7.6715	8.6307	0.51889	0.94431	1.1848
50	4.8982	6.3915	6.9751	0.50954	0.78901	0.99334
75	4.5724	5.4352	5.7578	0.50348	0.47608	0.56004
100	4.3699	4.8232	4.9835	0.54370	0.39405	0.41644

Table 5
Variation in kinetic energy against (β) and (Ha).

K. E			
Ha	$\beta=0.1$	$\beta=1$	$\beta=10$
0	148.31	1370.6	2534.6
25	107.34	543.65	765.81
50	55.878	168.55	204.11
75	27.729	63.363	72.620
100	13.934	26.755	29.750

Conclusion

The prime objective of this work is to adumbrate characteristics of thermal and solutal convection in Casson fluid enclsosed in star cavity with corrugations. Additionally, rectangular plate of unit length is adjusted in the domain and uniform thermal and solutal distributions are provided. Formulation of problem is conceded in the form of dimensionless equations and solve numerically by finite element based commercial software (COMSOL). Some salient key findings are enlisted below.

i) Decrementing trend in velocity is observed against Hartmann number (Ha) due to generation of resistive forces in the domain.
ii) At lower values of Casson parameter (β) velocity as well as kinetic energy exhibits decreasing aspects.
iii) Rayleigh number (Ra) causes uplift in temperature distribution whereas the concentration profile depcricates.
iv) Lewis number (Le) has inverse relation with mass diffusivity and no prominent effect on velocity and temperature fields.
v) Intensification in kinetic energy is revealed against (Ha) whereas contrary attribute is observed against (β).
vi) Heat and mass flux coefficients show diminishing aspects against Hartmann number (Ha).
vii) Heat and mass flux distribution exhibit upsurging behaviour against Casson parameter (β).

CRediT authorship contribution statement

Imtiaz Ali Shah: Conceptualization, Writing – original draft. **S. Bilal:** Methodology. **Arshad Riaz:** Writing – review & editing, Investigation. **ElSayed M. Tag El-Din:** Funding acquisition, Software. **M.M. Alqarni:** Validation. **Haneen Hamam:** Validation, Methodology.

Declaration of Competing Interest

The authors declare that they have no known competing financial interests or personal relationships that could have appeared to influence the work reported in this paper.

Data availability

Data will be made available on request.

Acknowledgement

The authors extend their appreciation to the Deanship of Scientific Research at King Khalid University for funding this work through Large Groups" .(Project under grant number (RGP.2/116/43)).

References

[1] Kefayati GHR, Tang H. Three-dimensional Lattice Boltzmann simulation on thermosolutal convection and entropy generation of Carreau-Yasuda fluids. Int J Heat Mass Transf 2019;131:346–64.
[2] Xin S, Le Quéré P, Tuckerman LS. Bifurcation analysis of double-diffusive convection with opposing horizontal thermal and solutal gradients. Phys Fluids 1998;10:850–8.
[3] Sezai I, Mohamad AA. Double diffusive convection in a cubic enclosure with opposing temperature and concentration gradients. Phys Fluids 2000;12:2210–23.
[4] Kuznetsov GV, Sheremet MA. A numerical simulation of double-diffusive conjugate natural convection in an enclosure. Int J Therm Sci 2011;50:1878–86.
[5] Khezzar L, Siginer D, Vinogradov I. Natural convection of power law fluids in inclined cavities. Int J Therm Sci 2012;53:8–17.
[6] Ali L, Ali B, Liu X, Ahmed S, Shah MA. Analysis of bio-convective MHD Blasius and Sakiadis flow with Cattaneo-Christov heat flux model and chemical reaction. Chin J Phys 2022;77:1963–75.
[7] Huppert HE, Stewart Turner J. Double-diffusive convection. J Fluid Mech 1981;106:299–329.
[8] Ostrach S. Fluid mechanics in crystal growth-the 1982 freeman scholar lecture. ASME J Fluids Eng 1983;105:5–20.
[9] Schmitt RW. Double diffusion in oceanography. Annu Rev Fluid Mech 1994;26(1):255–85.
[10] Radko T. Double-diffusive convection. Cambridge University Press; 2013.
[11] Corcione M, Grignaffini S, Quintino A. Correlations for the double-diffusive natural convection in square enclosures induced by opposite temperature and concentration gradients. Int J Heat Mass Transf 2015;81:811–9.
[12] Beghein C, Haghighat F, Allard F. Numerical study of double-diffusive natural convection in a square cavity. Int J Heat Mass Transf 1992;35:833–46.
[13] Gobin D, Bennacer R. Cooperating thermosolutal convection in enclosures—II. Heat transfer and flow structure. Int J Heat Mass Transf 1996;39:2683–97.
[14] Al-Amiri AM, Khanafer KM, Pop I. Numerical simulation of combined thermal and mass transport in a square lid-driven cavity. Int J Therm Sci 2007;46:662–71.
[15] Zhou P, Zhong Y, Wang H, Fan L, Licheng Dong Fu, Li QL, et al. Behavior of Fe/nano-Si particles composite electrodeposition with a vertical electrode system in a static parallel magnetic field. Electrochim Acta 2013;111:126–35.
[16] Chen S, Tölke J, Krafczyk M. Numerical investigation of double-diffusive (natural) convection in vertical annuluses with opposing temperature and concentration gradients. Int J Heat Fluid Flow 2010;31:217–26.
[17] Kefayati GHR, Tang H. Double-diffusive natural convection and entropy generation of Carreau fluid in a heated enclosure with an inner circular cold cylinder (Part I: heat and mass transfer). Int J Heat Mass Transf 2018;120:731–50.
[18] Kefayati G. Lattice Boltzmann simulation of double-diffusive natural convection of viscoplastic fluids in a porous cavity. Phys Fluids 2019;31(1):013105.
[19] Kefayati GHR. Thermosolutal natural convection of viscoplastic fluids in an open porous cavity. Int J Heat Mass Transf 2019;138:401–19.
[20] Qin Q, Xia ZA, Tian ZF. High accuracy numerical investigation of double-diffusive convection in a rectangular enclosure with horizontal temperature and concentration gradients. Int J Heat Mass Transf 2014;71:405–23.
[21] Selimefendigil F, Öztop HF. Magnetohydrodynamics forced convection of nanofluid in multi-layered U-shaped vented cavity with a porous region considering wall corrugation effects. Int Commun Heat Mass Transfer 2020;113:104551.
[22] Selimefendigil F, Chamkha AJ. Magnetohydrodynamics mixed convection in a power law nanofluid-filled triangular cavity with an opening using Tiwari and Das' nanofluid model. J Therm Anal Calorim 2019;135:419–36.
[23] Selimefendigil F, Öztop HF. Hydro-thermal performance of CNT nanofluid in double backward facing step with rotating tube bundle under magnetic field. Int J Mech Sci 2020;185:105876.
[24] Shoeibi S, Rahbar N, Esfahlani AA, Kargarsharifabad H. Application of simultaneous thermoelectric cooling and heating to improve the performance of a solar still: an experimental study and exergy analysis. Appl Energy 2020;263:114581.
[25] Fares R, Mebarek-Oudina F, Aissa A, Bilal SM, Öztop HF. Optimal entropy generation in Darcy-Forchheimer magnetized flow in a square enclosure filled with silver based water nanoliquid. *J Therm Anal Calorimetry* 2022;147:1571–81.
[26] Casson N. "A flow equation for pigment-oil suspensions of the printing ink type." *Rheology of disperse systems* (1959).
[27] Subba Rao A, Ramachandra Prasad V, Bhaskar Reddy N, Anwar Bég O. Heat transfer in a Casson rheological fluid from a semi-infinite vertical plate with partial slip. Heat Transfer—Asian Research 2015;44:272–91.
[28] Bird,, Byron R, Dai GC, Yarusso BJ. The rheology and flow of viscoplastic materials. Rev Chem Eng 1983;1:1–70.
[29] Mitsoulis E. "Flows of viscoplastic materials: models and computations Rheol." (2007): 135-78.
[30] Hayat T, Shehzad SA, Alsaedi A. Soret and Dufour effects on magnetohydrodynamic (MHD) flow of Casson fluid. Appl Math Mech 2012;33:1301–12.
[31] Öztop HF, Estellé P, Yan W-M, Al-Salem K, Orfi J, Mahian O. A brief review of natural convection in enclosures under localized heating with and without nanofluids. Int Commun Heat Mass Transfer 2015;60:37–44.
[32] Mustafa M, Hayat T, Pop I, Aziz Al. Unsteady boundary layer flow of a Casson fluid due to an impulsively started moving flat plate. Heat Transfer—Asian Res 2011;40:563–76.
[33] Animasaun IL. Effects of thermophoresis, variable viscosity and thermal conductivity on free convective heat and mass transfer of non-darcian MHD dissipative Casson fluid flow with suction and nth order of chemical reaction. J Nigerian Math Soc 2015;34:11–31.
[34] Garandet JP, Alboussiere T, Moreau R. Buoyancy driven convection in a rectangular enclosure with a transverse magnetic field. Int J Heat Mass Transf 1992;35:741–8.
[35] Rudraiah N, Barron RM, Venkatachalappa M, Subbaraya CK. Effect of a magnetic field on free convection in a rectangular enclosure. Int J Eng Sci 1995;33:1075–84.
[36] Hadid HB, Henry D. Numerical simulation of convective three-dimensional flows in a horizontal cylinder under the action of a constant magnetic field. J Cryst Growth 1996;166:436–45.
[37] Tagawa T, Ozoe H. Enhancement of heat transfer rate by application of a static magnetic field during natural convection of liquid metal in a cube. 1997: 265-71.
[38] Sheremet MA, Oztop HF, Pop I. MHD natural convection in an inclined wavy cavity with corner heater filled with a nanofluid. J Magn Magn Mater 2016;416:37–47.
[39] Kefayati GH. Lattice Boltzmann simulation of natural convection in a nanofluid-filled inclined square cavity at presence of magnetic field. Sci Iran 2013;20(5):1517–27.
[40] Kefayati GHR, Tang H. MHD mixed convection of viscoplastic fluids in different aspect ratios of a lid-driven cavity using LBM. Int J Heat Mass Transf 2018;124:344–67.
[41] Akram J, Akbar NS, Tripathi D. A theoretical investigation on the heat transfer ability of water-based hybrid (Ag–Au) nanofluids and Ag nanofluids flow driven by electroosmotic pumping through a microchannel. Arab J Sci Eng 2021;46(3):2911–27.
[42] Akram J, Akbar NS, Tripathi D. Comparative study on ethylene glycol based Ag-Al2O3 and Al2O3 nanofluids flow driven by electroosmotic and peristaltic pumping: a nano-coolant for radiators. Phys Scr 2020;95(11):115208.
[43] Tripathi D, Prakash J, Bég OA. Peristaltic pumping of hybrid nanofluids through an asymmetric microchannel in the presence of electromagnetic fields. *J Therm Sci Eng Appl* 2020.
[44] Prakash J, Tripathi D, Anwar Bég O. "Comparative study of hybrid nanofluids in microchannel slip flow induced by electroosmosis and peristalsis. Appl Nanosci 2020;10(5):1693–706.
[45] Prakash J, Gnaneswara Reddy M, Tripathi D, Tiwari AK. A model for electro-osmotic flow of pseudoplastic nanofluids in presence of peristaltic pumping: an

application to smart pumping in energy systems. In: Nanotechnology for Energy and Environmental Engineering. Cham: Springer; 2020. p. 185–213.
[46] Akbar NS, Abid SA, Tripathi D, Mir NA. Nanostructures study of CNT nanofluids transport with temperature-dependent variable viscosity in a muscular tube. Eur Phys J Plus 2017;132(3):1–10.
[47] Siddiqui AM, Farooq AA, Rana MA. A mathematical model for the flow of a Casson fluid due to metachronal beating of cilia in a tube. Sci World J 2015;2015.
[48] Hussain S, Shoeibi S, Armaghani T. Impact of magnetic field and entropy generation of Casson fluid on double diffusive natural convection in staggered cavity. Int Commun Heat Mass Transfer 2021;127:105520.